Intrazeolite Anchoring of Platinum Carbonyl Dianion Clusters: Synthesis, Characterization, and Their Catalytic Performances

James G.-C. Shen[†]

Lash Miller Chemical Laboratories, Department of Chemistry, University of Toronto, 80 St George Street, Toronto, Ontario, M5S 3H6 Canada

Received: March 30, 1999; In Final Form: September 24, 1999

This paper focuses on the intra-zeolite anchoring of platinum carbonyl dianion clusters and their catalytic performances. The synthesis involves the dispersion of $PtCl_2$ vapor followed by reductive carbonylation under a mixed CO and H_2O or a CO atmosphere. The characterization of Pt carbonyl dianions was based on a multianalytical approach including powder X-ray diffraction (PXRD), infrared spectroscopy, CO/H_2 gas chemisorption, ^{13}CO isotopic exchange, NO interaction, and reversible decarbonylation. The results provide an informative picture for the formation of the intra-zeolite anchoring of $[Pt_3(CO)_3(\mu_2\text{-}CO)_3]_n^{2-}$ ($n = 3$ or 4) dianions. $[Pt_3(CO)_3(\mu_2\text{-}CO)_3]_4^{2-}$ can be converted into $[Pt_3(CO)_3(\mu_2\text{-}CO)_3]_3^{2-}$ under a H_2O or H_2 atmosphere. The decarbonylated $[Pt_3(CO)_3(\mu_2\text{-}CO)_3]_4^{2-}/Na_{56}Y$ shows catalytic activity for methane homologation.

Introduction

The zeolite-mediated synthesis of organometallic provide a new route in comparison with conventional solution techniques. For example, several neutral and anionic intra-zeolitic metal carbonyl clusters have been recently reported, including Rh, Ir, Co, and Ru carbonyl clusters.[1] The catalytic activity of metallic carbonyl clusters usually requires decarbonylation in order to give close to structurally uniform materials that offer the prospect of being size and/or shape selective catalysts.[1−5] For the zeolitic $[Rh_6(CO)_{16}]$,[6] $[Ir_6(CO)_{16}]$,[7] $[Co_4(CO)_{12}]$,[4] $[Co_6(CO)_{16}]$,[8] $[Ru_6(CO)_{18}]$,[2−9] and $[HCoRu_3(CO)_{13}]$,[10] reversible decarbonylation and recarbonylation took place, which suggests that their metallic framework remains constant.

Zeolite-supported small platinum clusters have extensive application and scientific value; e.g., Pt clusters with as few as 5 or 6 atoms encapsulated in the cavities of basic zeolite L (containing K^+ and Ba^{2+} exchange ions) show active and stable catalysis for naphtha reforming for production of aromatics.[11,12] Highly selective catalysis is associated with the smaller cluster (less than 10 Å).[1−4] The nanocavities of zeolites favor entrapment of clusters.[6−10] In this regard, our work focuses on finding an improved method for the synthesis of Pt carbonyl dianion clusters inside the $Na_{56}Y$ cages, and the physicochemical characterization through a multianalytical approach, including infrared spectroscopy, CO and H_2O chemisorption, and NO interaction. Methane homologation was carried out on the zeolitic Pt clusters.

Results

1. Characterization of the Intra-zeolite Anchoring of Platinum Carbonyl Dianions by Power X-ray Diffraction and Infrared Spectroscopy. *Vapor Dispersion of $PtCl_2$ in $Na_{56}Y$ Zeolite Cavities.* The zeolite-supported $PtCl_2$ (12 wt % Pt loading or 6 Pt atoms/unit cell) was characterized through PXRD. This pattern shows PXRD reflections at $2\theta = 12.7°$, 13.5°, 22.0°, 23.5°, 27.4°, 30.4°, 35.4°, and 51.5° (Figure 1, trace a) ascribed to crystalline $PtCl_2$. Traces b, c, and d of Figure 1 show diffraction patterns of the heated mixture of $PtCl_2$ and $Na_{56}Y$ zeolite at 300 K (trace b), at 473 K, 36 h (trace c), and at 473 K, 60 h (trace d). The intensity of crystalline PtC_2 patterns decreases with increasing temperature and time. After 98 h of heating at 473 K, the PXRD reflections for $PtCl_2$ completely disappeared, leaving only the PXRD peaks for $Na_{56}Y$ (traces e). This suggests that $PtCl_2$ is highly dispersed in the $Na_{56}Y$ cavities. In addition, the introduction of more than 6 moles of $PtCl_2$ per unit cell has caused crystalline $PtCl_2$ at the heating temperature employed (diffraction pattern in Figure 1, trace a) and crystalline metallic Pt to form (PXRD, $2\theta = 39.7°$ and 46.1° of Figure 1) at higher temperature such as 523 K. Six moles of $PtCl_2$ per unit cell seemed to be the maximum amount of $PtCl_2$ adsorbed in the $Na_{56}Y$ cavities.

Sample a. Figure 2 shows the in situ infrared spectra in the reaction of $Pt^{2+}/Na_{56}Y$ with 550 Torr of CO and 15 Torr of H_2O at 298−353 K. Upon exposure to a mixed CO and H_2O atmosphere at 298 K, the CO bands appear at 2112, 1894, and 1845 cm^{-1} (Figure 2, part B, trace a). The intensity of these bands successively increases with increasing temperature and time (Figure 2, part B, traces b−e). When the temperature reached 333 K, the band at 1894 cm^{-1} remained constant, but the 2112 cm^{-1} band shifted to 2080 cm^{-1}, the 1845 cm^{-1} band shifted to 1824 cm^{-1}, and a new band appeared at 1860 cm^{-1} (Figure 2, part B, trace f). These four infrared bands at 2080, 1894, 1860, and 1824 cm^{-1} grew with increasing temperature and time (Figure 2, part B, traces f−h). After 8 h of heating at 353 K, these bands reached their maximum intensities (Figure 2, part B, trace i, and Table 1). Despite differences in the amplitudes of peaks, the CO infrared bands of the resulting sample at 2080 (vs) and 1824 (s) cm^{-1} resemble bands (2040 (vs) and 1860 (s) cm^{-1}) of $[Pt_3(CO)_3(\mu_2\text{-}CO)_3]_4^{2-}$ dianion in tetrahydrofuran (THF) solution (Figure 2, part C).[13,14] On the other hand, the bands at 2112 (s), 1894 (s), and 1860 (m) cm^{-1} of the resulting spectrum (Figure 2, part B, trace i) are analogous with bands (2030 (vs), 1840 (s), and 1810 (m) cm^{-1}) of $[Pt_3(CO)_3(\mu_2\text{-}CO)_3]_3^{2-}$ dianion in THF solution (Figure 2, part D)][14]

[†] Present address: Department of Chemical Engineering and Materials Science, University of California, Davis, CA 95616. E-mail: jgcshen50@hotmail.com.

10.1021/jp991095y CCC: $19.00
Published on Web 12/28/1999

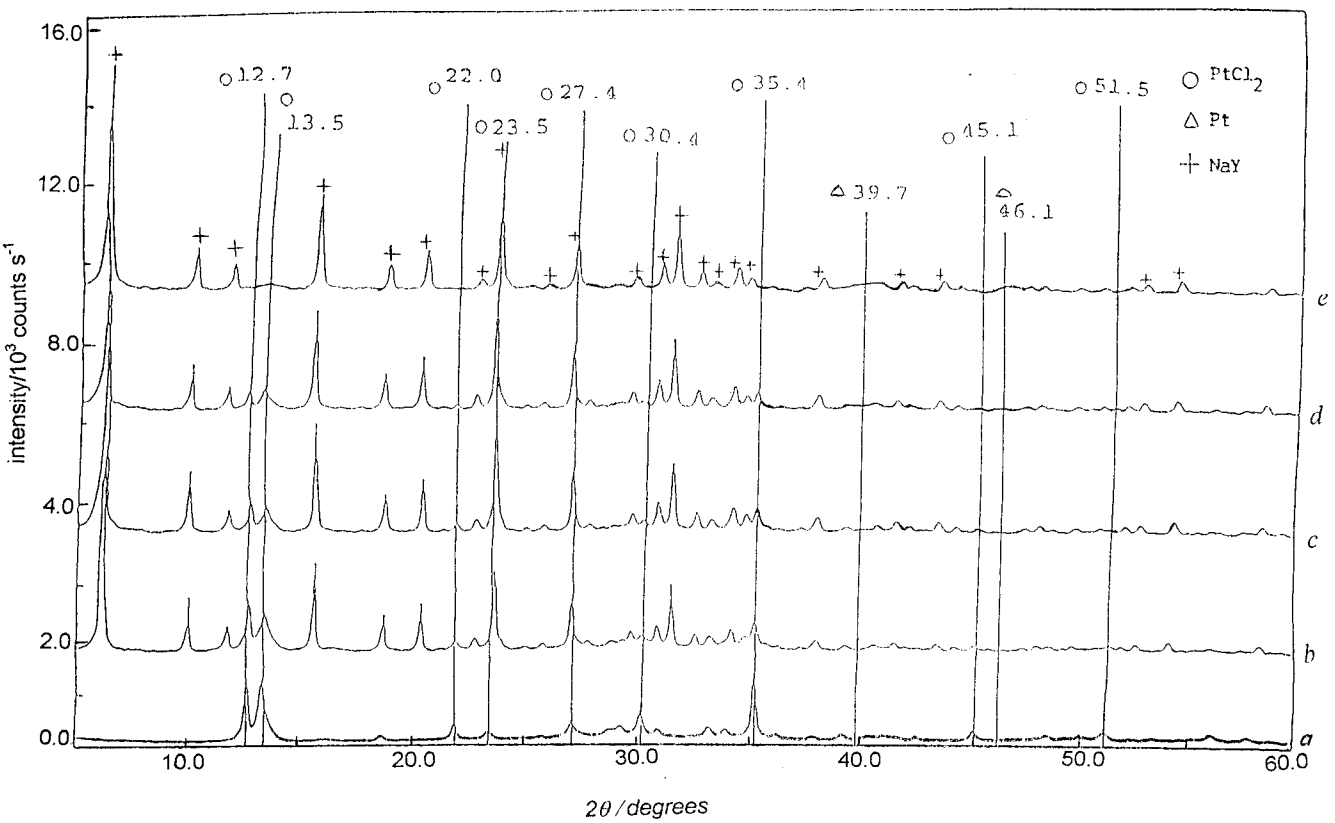

Figure 1. PXRD patterns of (trace a) crystalline $PtCl_2$, (trace b) $PtCl_2$ mechanically mixed with $Na_{56}Y$ at 298 K under a N_2 atmosphere, (trace c) the mixture was heated at 473 K for 36 h, (trace d) at 473 K for 60 h, and (trace e) at 473 K for 98 h.

but with a shift of carbonyl bands. The relative abundance of $[Pt_3(CO)_3(\mu_2\text{-}CO)_3]_4^{2-}$ and $[Pt_3(CO)_3(\mu_2\text{-}CO)_3]_3^{2-}$ species of sample a was calculated from the areas of the bridging CO band at 1824 cm^{-1} for $[Pt_3(CO)_3(\mu_2\text{-}CO)_3]_4^{2-}$ and the bridging CO band at 1894 cm^{-1} for $[Pt_3(CO)_3(\mu_2\text{-}CO)_3]_3^{2-}$ species, where we assumed equal extinction coefficients of CO_b for $[Pt_3(CO)_3(\mu_2\text{-}CO)_3]_4^{2-}$ and $[Pt_3(CO)_3(\mu_2\text{-}CO)_3]_3^{2-}$ species. The result is 70% $[Pt_3(CO)_3(\mu_2\text{-}CO)_3]_4^{2-}$ and 30% $[Pt_3(CO)_3(\mu_2\text{-}CO)_3]_3^{2-}$. In addition, it is notable that corresponding to the increase of CO band intensities (Figure 2, part B, traces a−i), the infrared bands of the bridged hydroxyl grow in intensities during the formation of the sample a (Figure 2, part A, traces a−i). The dark green of the sample a differs from the blue-green color of crystalline $[Pt_3(CO)_3(\mu_2\text{-}CO)_3]_4^{2-}$.[13−15] This may be ascribed to the fact that the sample a is a mixture of $[Pt_3(CO)_3(\mu_2\text{-}CO)_3]_4^{2-}$ (blue-green) and $[Pt_3(CO)_3(\mu_2\text{-}CO)_3]_3^{2-}$ (violet-red) in the $Na_{56}Y$ cavities (Table 2).

Sample b. Figure 3 shows the in situ infrared spectra in the reaction of $Pt^{2+}/Na_{56}Y$ with 550 Torr of CO at 298−353 K. Here, the same temperature-programmed heating was used as for sample a. At 298−323 K, the four infrared bands at 2078, 1896, 1866, and 1827 cm^{-1} increase with increasing temperature and time. When the temperature reaches beyond 323 K, the bands at 2078 and 1827 cm^{-1} continuously increase, whereas the bands at 2112, 1896, and 1866 cm^{-1}, due to $[Pt_3(CO)_3(\mu_2\text{-}CO)_3]_3^{2-}$, decrease (Figure 3, traces e−k). The resulting infrared spectrum record only shows bands at 2080 (vs) and 1824 (s) cm^{-1}, which is accompanied by the synthesis of pure $[Pt_3(CO)_3(\mu_2\text{-}CO)_3]_4^{2-}$ dianion (trace k). Sample b reveals a blue-green color, in agreement with crystalline $[Pt_3(CO)_3(\mu_2\text{-}CO)_3]_4^{2-}$ dianion (Table 2).[13−15]

Sample c. We record the in situ infrared spectra with introduction of 100 Torr of H_2 into sample b in infrared cell. Infrared bands at 2080 and 1824 cm^{-1}, assigned to $[Pt_3(CO)_3(\mu_2\text{-}CO)_3]_4^{2-}$, decrease, whereas bands at 1894 and 1860 cm^{-1}, ascribed to $[Pt_3(CO)_3(\mu_2\text{-}CO)_3]_3^{2-}$, grow with increasing temperature and time, where the 2112 cm^{-1} band of $[Pt_3(CO)_3(\mu_2\text{-}CO)_3]_3^{2-}$ species is expected to overlap with a huge band at 2080 cm^{-1} (Figure 4). These bands are similar to CO bands observed in sample a. The resulting infrared spectrum (Figure 4, trace f) is analogous to the spectrum of Figure 2, part A, trace f. Thus, this is consistent with the inference that sample c involves a mixture of $[Pt_3(CO)_3(\mu_2\text{-}CO)_3]_4^{2-}$ and $[Pt_3(CO)_3(\mu_2\text{-}CO)_3]_3^{2-}$ dianions, with the dodecaplatinum carbonyl dianion being the dominant species.

When organometallic species were extracted from the synthetic samples a or b in an acetone solution of *n*-Bu_4NBr, the solution remained colorless and showed no infrared absorption in the CO stretching region. Further, no appreciable CO frequency shifts were observed when crystalline $[Pt_3(CO)_3(\mu_2\text{-}CO)_3]_4^{2-}$ or $[Pt_3(CO)_3(\mu_2\text{-}CO)_3]_3^{2-}$ was deposited from the organic solution onto the $Na_{56}Y$ zeolite wafer.

2. ^{13}CO Isotopic Exchange Reaction, and Decarbonylation−Recarbonylation of $[Pt_3(CO)_3(\mu_2\text{-}CO)_3]_4^{2-}/Na_{56}Y$. On exposure of sample a to ^{13}CO of 50 Torr at 313 K, the bands at 2112, 1894, and 1860 cm^{-1}, assigned to $[Pt_3(CO)_3(\mu_2\text{-}CO)_3]_3^{2-}$ dianion were rapidly exchanged to give new bands at 2060, 1855, and 1822 cm^{-1} (not shown). In contrast, the reaction proceeds very slowly on ^{13}CO gas with $[Pt_3(CO)_3(\mu_2\text{-}CO)_3]_4^{2-}$ in sample b. After 6 h at 340 K, the terminal CO band at 2080 cm^{-1} was replaced by 2028 cm^{-1}, while the bridging CO band at 1824 cm^{-1} was substituted by a new band at 1779 cm^{-1} (Figure 5, part b). The values of the band shifts after isotopic exchange by 50−60 cm^{-1} roughly are in the range calculated according to the two-atom model ($\Delta\nu = 44$ cm^{-1}).[9] The stepwise reaction of ^{13}CO isotopic exchange at 313−340 K further confirms that sample a contained two-clusters species,[8] and the $[Pt_3(CO)_3(\mu_2\text{-}CO)_3]_3^{2-}$ may be an intermediate of $[Pt_3$-

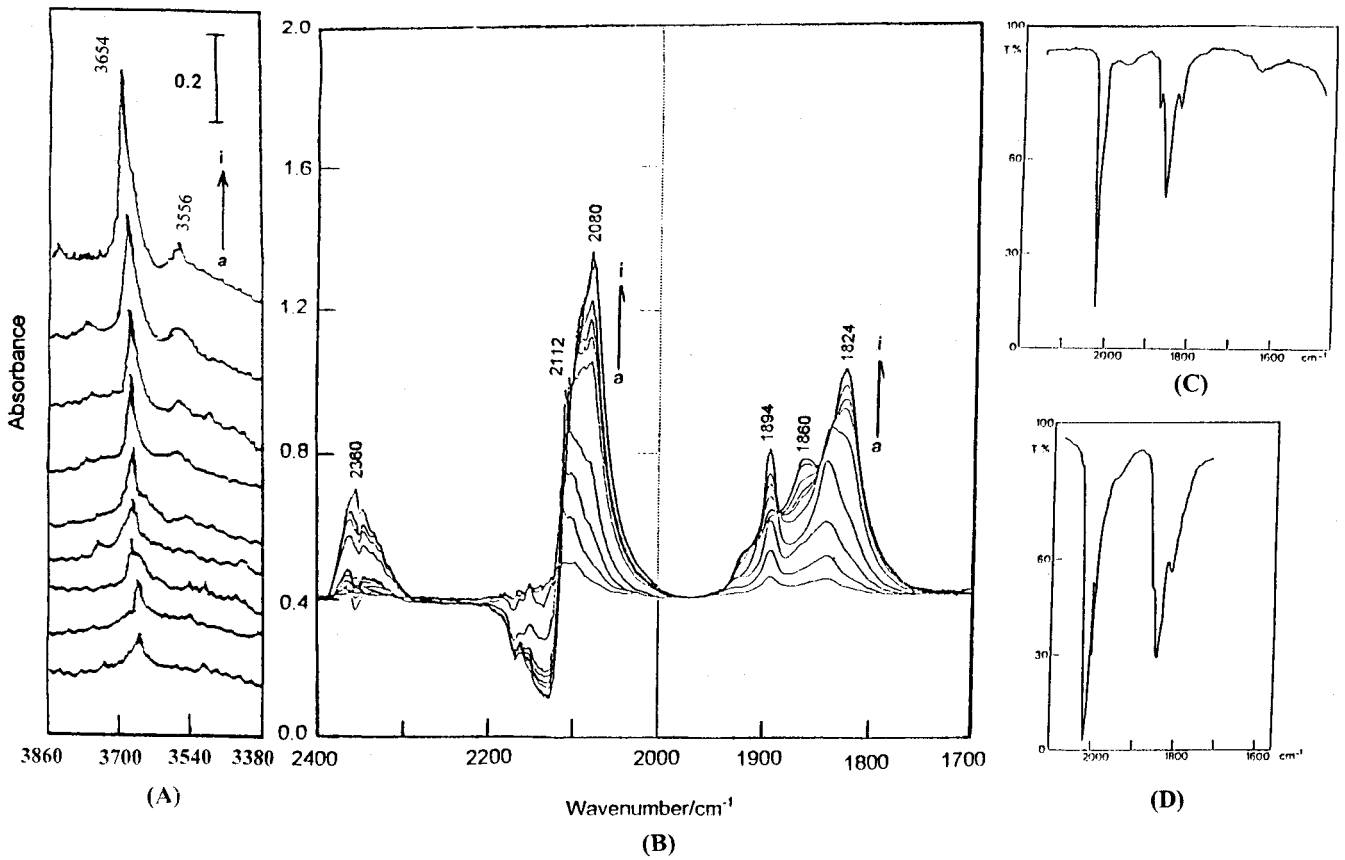

Figure 2. In situ infrared spectra of reductive carbonylation of $Pt^{2+}/Na_{56}Y$ by 550 Torr of CO and 15 Torr of H_2O at 298−353 K: (trace a) 298 K, 20 min; (trace b) 333 K, 20 min; (trace c) 333 K, 1 h; (trace d) 333 K, 2 h; (trace e) 353 K, 10 min; (trace f) 353 K, 30 min; (trace g) 353 K, 1 h; (trace h) 353 K, 3 h; (trace i) 353 K, 8 h.

TABLE 1: Carbonyl Infrared Stretching Frequencies of Samples and Assignment

samples	CO FT-IR bands/cm^{-1}	assignment
sample a[a]	2110 (s), 2080 (vs), 1894 (s), 1860 (s), 1824 (vs)	$[Pt_3(CO)_3(\mu_2\text{-}CO)_3]_4^{2-}/Na_{56}Y$ $[Pt_3(CO)_3(\mu_2\text{-}CO)_3]_3^{2-}/Na_{56}Y$
sample b[a]	2078 (vs), 1827 (s)	$[Pt_3(CO)_3(\mu_2\text{-}CO)_3]_4^{2-}/Na_{56}Y$
sample c[a]	2080 (vs), 1898 (m), 1864 (s), 1823 (s)	$[Pt_3(CO)_3(\mu_2\text{-}CO)_3]_4^{2-}/Na_{56}Y$ $[Pt_3(CO)_3(\mu_2\text{-}CO)_3]_3^{2-}/Na_{56}Y$
$[Pt_{12}(CO)_{24}]^{2-}/MgO$[b]	2048 (vs), 1862 (s)	$[Pt_3(CO)_3(\mu_2\text{-}CO)_3]_4^{2-}/MgO$

[a] This work. [b] Reference 19.

TABLE 2: Infrared[a] and UV−Vis[b] Spectra of $[Pt_3(CO)_3(\mu_2\text{-}CO)_3]_n$ ($n = 1-6$) in THF Solution

cluster	ν_{CO}/cm^{-1}	λ_{max}/nm	color
$[Pt_3(CO)_3(\mu_2\text{-}CO)_3]_6^{2-}$	2065(vs), 1900(sh), 1875(s) 1855(sh), 1840(sh)	720	olive-green
$[Pt_3(CO)_3(\mu_2\text{-}CO)_3]_5^{2-}$	2055(vs), 1890(mw), 1870(s) 1840(sh), 1830(sh)	700	yellow-green
$[Pt_3(CO)_3(\mu_2\text{-}CO)_3]_4^{2-}$	2040(vs), 2030(sh), 1880(mw) 1860(s), 1825(mw)	620, 392	blue-green
$[Pt_3(CO)_3(\mu_2\text{-}CO)_3]_3^{2-}$	2030(vs), 1855(sh), 1840(s) 1830(sh), 1810(m)	560, 368	violet-red
$[Pt_3(CO)_3(\mu_2\text{-}CO)_3]_2^{2-}$	1995(vs), 1818(m), 1795(s)		orange-red
$[Pt_3(CO)_3(\mu_2\text{-}CO)_3]^{2-}$	1945(vs), 1740(s)		pink-red

[a] Reference 14. [b] Reference 15.

$(CO)_3(\mu_2\text{-}CO)_3]_4^{2-}$ dianion. In addition, when normal CO was introduced at 353 K, the infrared spectrum changed back to that observed initially (Figure 5, part a, and Figure 6, part B, circle a → c → a). This suggests there is no change in the metal skeleton of the zeolitic platinum carbonyl dianions during isotopic exchange.

Sample b was evacuated under 10^{-5} Torr of vacuum at a heating rate of 5 K/min, from 298 to 423 K. The 2080 (vs) and 1824 (s) cm^{-1} carbonyl bands remain at constant frequency but with a decrease of peak intensity. Upon heating the sample at 423 K for 30 min, the carbonyl bands completely disappeared, to give decarbonylated platinum intra-zeolite clusters ($[Pt_x]_{dec}/Na_{56}Y$, as shown in Figure 7, trace a and Figure 6, part A, b).

The decarbonylated species was recarbonylated through treatment with 150 Torr of CO at 298 K. Upon exposure of CO gas at 298 K, the infrared spectrum appears at 2080 and

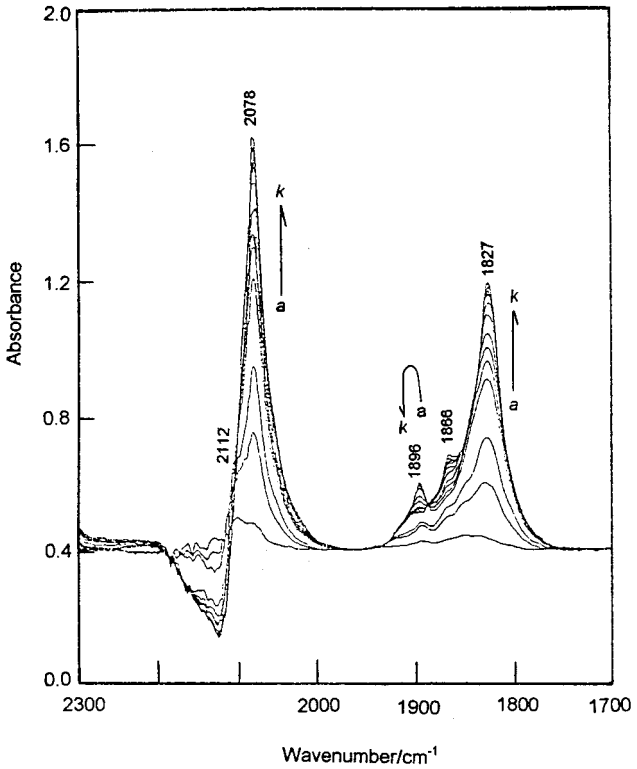

Figure 3. In situ infrared spectra of reductive carbonylation of Pt^{2+}/$Na_{56}Y$ by 550 Torr of CO at 298−353 K: (trace a) 298 K, 10 min; (trace b) 333 K, 20 min; (trace c) 333 K, 40 min; (trace d) 333 K, 1 h; (trace e) 353 K, 10 min; (trace f) 353 K, 30 min; (trace g) 353 K, 1 h; (trace h) 353 K, 2 h; (trace i) 353 K, 4 h; (trace j) 353 K, 6 h; (trace k) 353 K, 8 h.

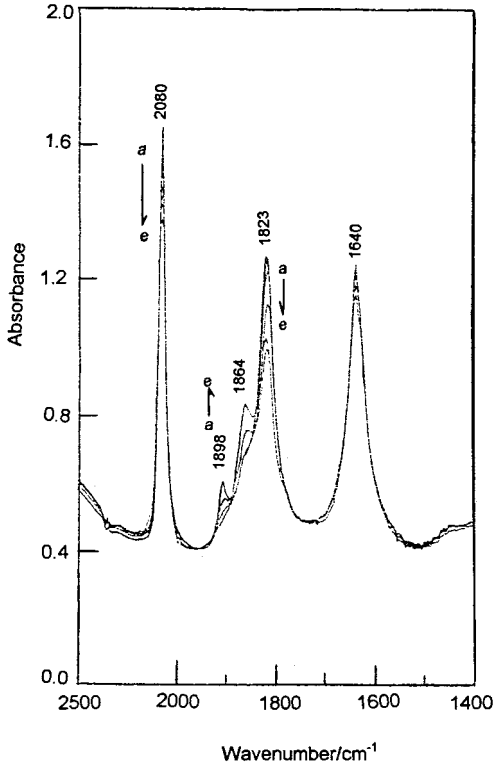

Figure 4. In situ infrared spectra of sample b under 100 Torr of H_2 at 298−373 K: (trace a) the sample b; (trace b) 298 K, 30 min; (trace c) 323 K, 30 min; (trace d) 353 K, 30 min; (trace e) 373 K, 30 min.

1824 cm^{-1} (Figure 7, trace b). The intensity of these two bands increases with the reaction time (Figure 7, traces c and d). The peaks in the infrared spectrum of the resulting sample (Figure

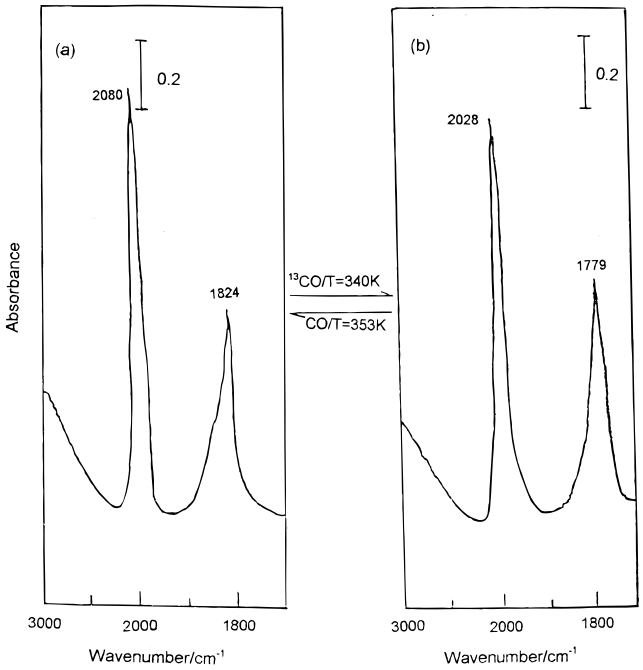

Figure 5. Infrared spectra obtained for (part a), sample b in a vacuum and (part b) ^{13}CO isotopic exchange of sample b under 50 Torr ^{13}CO atmosphere at 353 K for 6 h.

7, trace e) were analogous with those of $[Pt_3(CO)_3(\mu_2\text{-}CO)_3]_4^{2-}$/$Na_{56}Y$ (Figure 3, trace i). This provides an indication that $[Pt_3(CO)_3(\mu_2\text{-}CO)_3]_4^{2-}$ was reformed inside the $Na_{56}Y$ cages (Figure 6, part A, circle a → b → a). The decarbonylated sample thereby can be considered to be defined as $[Pt_{12}]_{dec}/Na_{56}Y$ (Figure 6, part A, b). It was found that the recarbonylated sample shows less peak intensity and full width at half-maximum (fwhm) as compared with the initial carbonylated Pt species in the sample b. When this process was carried out several times, the sample is typically gray and has a terminal CO band at 2020 cm^{-1} but no bridging CO band. This single peak is an indicative of CO adsorbed on metallic Pt particles, and the gray color is consistent with the presence of metal Pt.[16,17] Thus, it is reasonably considered that part of the metallic Pt skeletons was broken, associated with the release of the carbonyl ligands in each decarbonylation of the $[Pt_3(CO)_3(\mu_2\text{-}CO)_3]_4^{2-}/Na_{56}Y$.

3. NO Interaction with $[Pt_3(CO)_3(\mu_2\text{-}CO)_3]_4^{2-}/Na_{56}Y$. When NO (150 Torr) was introduced into the sample b wafer in an infrared cell at 298 K, the 2080 (vs) and 1824 (s) cm^{-1} carbonyl bands rapidly disappeared, and new carbonyl bands assigned to $[Pt_3(CO)_3(\mu_2\text{-}CO)_3]_3^{2-}$ appeared at 2112, 1900, and 1853 cm^{-1} (Figure 8, part b). In this reactive stage, $[Pt_3(CO)_3(\mu_2\text{-}CO)_3]_4^{2-}$ shows significant activity in comparison with its ^{13}CO isotopic reaction. Moreover, the gaseous products, N_2O (2236 cm^{-1}) and CO_2 (2353 cm^{-1}), appear in the infrared spectrum, followed by carbonate formation (1430 and 1340 cm^{-1}) (not shown).[18] The gaseous products were also detected through GC-MS. In further reaction with NO at 313 K for 2 h, the 1900 and 1853 cm^{-1} bands disappeared and a high-frequency band at 2110 cm^{-1} emerges (Figure 8, part c), which is attributed to the presence of a carbonyl ligand terminally bound to an oxidized platinum center.[19−21] The 2110 cm^{-1} peak is similar to the peak of PtO(CO) species which results from the CO and O_2 coadsorption on a Pt/Al_2O_3 catalyst.[22] When the PtO(CO) species reacted with CO at 353 K, the regeneration process occurred which is via the reductive carbonylation of PtO(CO) to $[Pt_3(CO)_3(\mu_2\text{-}CO)_3]_3^{2-}$ followed conversion to $[Pt_3(CO)_3(\mu_2\text{-}CO)_3]_4^{2-}$ dianions (Figure 6, part C, circle a → d → e → a).

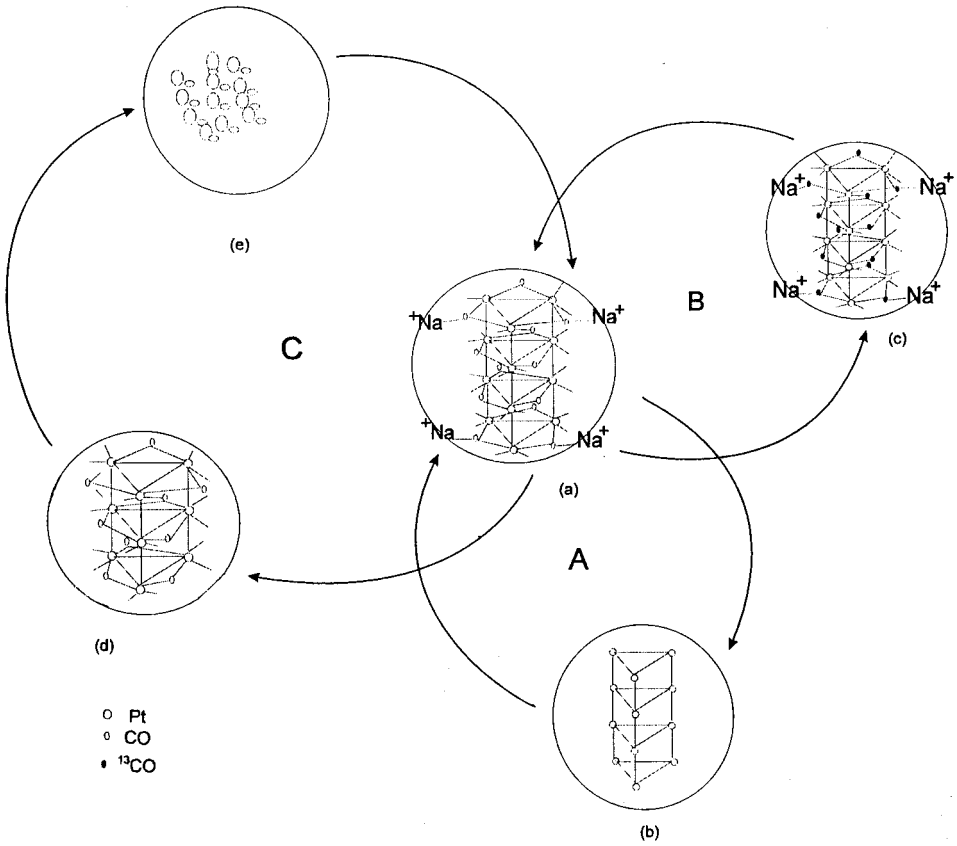

Figure 6. Scheme for the chemistry of the intra-zeolitic $[Pt_3(CO)_3(\mu_2\text{-}CO)_3]_4^{2-}$ dianion clusters: (A, circle a → b → a) the reversible decarbonylation and recarbonylation of $[Pt_3(CO)_3(\mu_2\text{-}CO)_3]_4^{2-}/Na_{56}Y$; (B, circle a → c → a) $^{13}CO/CO$ isotopic exchange reaction of $[Pt_3(CO)_3(\mu_2\text{-}CO)_3]_4^{2-}/Na_{56}Y$; (C, circle a → d → e → a) NO oxidation fragmentation and CO reductive regeneration for $[Pt_3(CO)_3(\mu_2\text{-}CO)_3]_4^{2-}/Na_{56}Y$.

The process is consistent with the reductive carbonylation of $Pt^{2+}/Na_{56}Y$ during a CO atmosphere.

4. Methane Homologation on the Intra-zeolite Anchoring of the Decarbonylated $[Pt_3(CO)_3(\mu_2\text{-}CO)_3]_4^{2-}$. Methane homologation has been developed in a two-step procedure by thermal dissociation of the methane on a supported metal catalyst, followed by hydrogenation of the surface species deposited on the catalyst.[3,4] The present well-defined and -characterized intra-zeolite anchoring of platinum clusters is considered to be an attractive catalyst with a large metallic surface area and small particle size in comparison with traditional bulk metal catalysts. Thus, they are expected to result in a favorable catalysis behavior for methane homologation.

Figure 9 shows temperature-programmed hydrogenation (TPH) plots of surface carbonaceous species from 20 μmol CH_4 dissociation at 623 K on the decarbonylated $[Pt_3(CO)_3(\mu_2\text{-}CO)_3]_4^{2-}/Na_{56}Y$ catalyst. The favorable hydrogenation temperature varies in terms of the size of hydrocarbon. The optimum hydrogenation temperatures of C_2, C_3, C_4, C_5, and C_6 hydrocarbon are 473, 573, 393, 453, and 573 K, respectively (Table 3). The C_2, C_3, C_4, C_5, and C_6 hydrocarbon fractions significantly display monotonic increases and decreases when T was set at lower and higher values than their optimum temperature, respectively. The selective catalysis of the reaction is remarkable, such as the production of a large amount of C_2 hydrocarbon but only a trace of C_3, C_4, and C_6 hydrocarbon at 473 K. At the optimum temperature for each hydrocarbon, the selectivity toward of C_2, C_3, C_4, C_5, and C_6 reached 67.8%, 1.8%, 43.2%, 17.6%, and 1.1%, respectively (Table 3). The region of hydrogenation temperature remarkably affected the yield of the C_{2+} hydrocarbons: for T = 393−543K, C_{2+} selectivity is >55%; for T < 393K, C_{2+} selectivity reaches 10%; for T > 543K, C_{2+} selectivity merely comes up to 7%; when T is increased beyond 673 K, the only product is C_1 and C_2. Moreover, it is interesting that the optimum C_3 temperature is higher than that of C_4 and C_5 (Figure 9 and Table 3). This implies that a part of the C_3 hydrocarbon would be created by hydrogenolysis and/or dissociation of the C_4 and C_5 hydrocarbon.

Discussion

1. Confirmation of $[Pt_3(CO)_3(\mu_2\text{-}CO)_3]_4^{2-}$ in $Na_{56}Y$ Zeolite Cavities. To confirm Pt carbonyl species in sample b, we represent Chini series Pt carbonyl dianion clusters (Table 2). $[Pt_3(CO)_3(\mu_2\text{-}CO)_3]_6^{2-}$ or $[Pt_3(CO)_3(\mu_2\text{-}CO)_3]_5^{2-}$ dianion is considered to be an unlikely candidate of sample b, because crystalline $[Pt_3(CO)_3(\mu_2\text{-}CO)_3]_6^{2-}$ shows the ν_{co} bands at 2065 (vs) and 1875 (s) cm^{-1}, while crystalline $[Pt_3(CO)_3(\mu_2\text{-}CO)_3]_5^{2-}$ shows the ν_{co} bands at 2055 (vs) and 1870 (s) cm^{-1} (Table 2).[13,14] Their terminal CO bands are located at lower frequencies in comparison with those of the sample b (2065 → 2080 cm^{-1} and 2055 → 2080 cm^{-1}), and the bridging CO bands are located at higher frequencies than those of the sample b (1870 → 1824 cm^{-1} and 1875 → 1824 cm^{-1}). The intra-zeolitic Pt carbonyl dianions are expected to show a blue shift of the terminal CO band and a red shift of the bridging CO band, which correspond with well-known ion-pairing effects.[2−5] Thus, $[Pt_3(CO)_3(\mu_2\text{-}CO)_3]_6^{2-}$ or $[Pt_3(CO)_3(\mu_2\text{-}CO)_3]_5^{2-}$ is not considered as "guests" located in $Na_{56}Y$ cavities. In contrast, the CO band shifts of $[Pt_3(CO)_3(\mu_2\text{-}CO)_3]_4^{2-}$ (ν_{cot} 2040 (vs) → 2080 (vs) cm^{-1} and ν_{cob} 1860 (s) → 1824 (s) $cm)^{-1}$ or $[Pt_3(CO)_3(\mu_2\text{-}CO)_3]_3^{2-}$ (ν_{tco} 2030 (vs) → 2080 (vs) cm^{-1} and ν_{bco} 1840 (s) → 1824 (s) $cm)^{-1}$ as "guests" entrapped in zeolite cages can match the infrared band shifts which caused from ion-pairing effects.[2−5] Further,

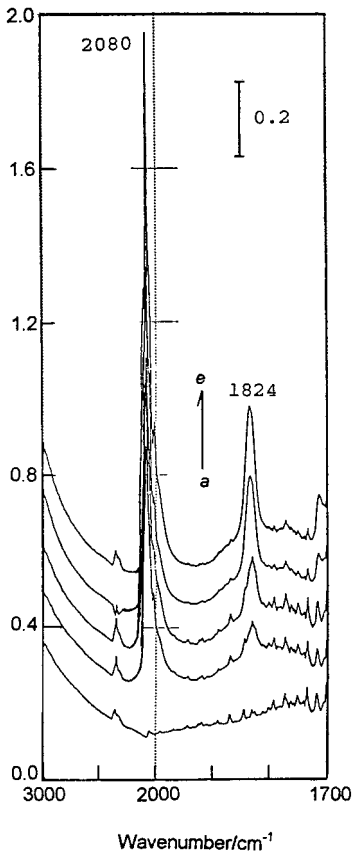

Figure 7. In situ infrared spectra characterizing samples: (trace a) the decarbonylated state of $[Pt_3(CO)_3(\mu_2\text{-}CO)_3]_4^{2-}/Na_{56}Y$ under 10^{-5} Torr vacuum at 423 K for 30 min; (trace b) the recarbonylation of the decarbonylated sample under 150 Torr of CO at 298 K for 5 min; (trace c) at 298 K for 2 h; (trace d) at 298 K for 4 h; and (trace e) at 298 K for 12 h.

the fitting magnitude of "guest" to "host" is discussed as follows. An approximate size of the Chini $[Pt_3(CO)_3(\mu_2\text{-}CO)_3]_n^{2-}$ dianions can be evaluated from the atomic distances determined.[14,15] For $n = 3$ the elliptical section is 8.43 × 9.40 Å, and the length of the pseudo-cylinder is 8.88 Å. For $n = 4$, 5, and 6, the elliptical section remains about 8.43 × 9.40 Å and the length of the pseudo-cylinder is 11.90, 15.10, and 18.18 Å, respectively, where we ignored 0.4−0.8 °C twisting deformations of the neighboring $Pt_3(CO)_3(\mu_2\text{-}CO)_3$. The α-cage of $Na_{56}Y$ is ca. 13 Å in diameter.[23] Thus, $n = 3$ or 4 type cluster can fit the α-cage. However, $[Pt_3(CO)_3(\mu_2\text{-}CO)_3]_5^{2-}$ and $[Pt_3(CO)_3(\mu_2\text{-}CO)_3]_6^{2-}$ are too large and can match the magnitude of $Na_{56}Y$ α-cage.

Chini $[Pt_3(CO)_3(\mu_2\text{-}CO)_3]_n^{2-}$ dianions with $n < 3$ are various shade of red.[13−15,24] In contrast, $[Pt_3(CO)_3(\mu_2\text{-}CO)_3]_4^{2-}$ is blue-green; $[Pt_3(CO)_3(\mu_2\text{-}CO)_3]_5^{2-}$ is yellow-green; and $[Pt_3(CO)_3(\mu_2\text{-}CO)_3]_6^{2-}$ is olive-green (Table 2).[14,15] Puga et al.[19] prepared MgO grafting $[Pt_3(CO)_3(\mu_2\text{-}CO)_3]_4^{2-}$ in blue-green color. The sample b with a high Pt content (12 wt %) shows blue-green. This is identical with that of Chini $[Pt_3(CO)_3(\mu_2\text{-}CO)_3]_4^{2-}$ dianion in THF solution or grafted on MgO surface, and rather different from violent-red of $[Pt_3(CO)_3(\mu_2\text{-}CO)_3]_3^{2-}$ in THF (Table 2)[14,15] or grafted on MgO surface.[19]

By this approach of deductive elimination, and the characterization of samples through the infrared spectra, the suggestion is consistent with the THF solution chemistry of $[Pt_3(CO)_3(\mu_2\text{-}CO)_3]_4^{2-}$, which took place in the reaction of CO and Pt^{2+} ions in the $Na_{56}Y$ cavities at 353 K.

2. Details of the Anchoring Site of Platinum Carbonyl Dianion Clusters inside the $Na_{56}Y$ α-Cages. The structure of $[Pt_3(CO)_3(\mu_2\text{-}CO)_3]_4^{2-}$ dianions is based on distorted D_{3h} geometry, with 12 Pt atoms forming prisms, each Pt bound to two terminal CO ligands, and two Pt atoms bound to one bridging CO ligand (Figure 6, part A, a).[13,14] One may doubt if platinum carbonyl clusters form on the external surface of $Na_{56}Y$ zeolite. The $[Pt_3(CO)_3(\mu_2\text{-}CO)_3]_4^{2-}$ can be extracted into solution from its state grafted on the MgO surface through an acetone solution of n-Bu_4NBr, in which the Br^- anions ion-exchange with the dianion clusters.[19] However, when platinum carbonyl species were extracted from the synthetic sample a or b using a solution of n-Bu_4NBr in acetone, the solution remained colorless. The results of the work here suggest that virtually all the platinum carbonyl clusters were formed and confined to the $Na_{56}Y$ cages. The synthetic $[Pt_3(CO)_3(\mu_2\text{-}CO)_3]_4^{2-}$ is small enough to fit inside α-cages but too large to match β-cage and hexagonal prism, and to diffuse through the apertures. When the crystalline $[Pt_3(CO)_3(\mu_2\text{-}CO)_3]_4^{2-}$ deposits on the external surface of $Na_{56}Y$ zeolite, no CO band shifts occurred. The process of decarbonylation and recarbonylation for $[Pt_3(CO)_3(\mu_2\text{-}CO)_3]_4^{2-}/Na_{56}Y$ can be performed (Figure 7 and Figure 6, part A, circle a → b → a). These data provide further evidence for the intra-zeolite anchoring of $[Pt_3(CO)_3(\mu_2\text{-}CO)_3]_4^{2-}$. The decarbonylation of MgO-supported $[Pt_3(CO)_3(\mu_2\text{-}CO)_3]_4^{2-}$ led to aggregation of platinum, loss of the structural integrity, and thereby no regeneration.[19] In this same vein, assuming the formation of Pt carbonyl dianion clusters on the extra-zeolite, the reversible re-formation of $[Pt_3(CO)_3(\mu_2\text{-}CO)_3]_4^{2-}$ resulting from CO chemisorption on its decarbonylated state will be unsuccessful since the extra-zeolitic Pt cluster coalesces under our severe decarbonylation condition. On the basis of this analysis, we suggest that the zeolite channels, with limited sizes, probably prevent Pt species within α-cages from coalescing and the internal topology of the α-cage is likely to play a significant role in the stabilization of Pt carbonyl dianion clusters.

The MgO-grafted $[Pt_3(CO)_3(\mu_2\text{-}CO)_3]_4^{2-}$ shows practically no infrared band shifts as compared with the crystalline $[Pt_3(CO)_3(\mu_2\text{-}CO)_3]_4^{2-}$ (ν_{cot} 2048 (vs) → 2040 (vs) cm^{-1}, and ν_{cob} 1862 (s) → 1860 (s) cm^{-1}) (Tables 1 and 2).[19] In contrast, the stretching frequency of the bridging CO ligands of the intra-zeolitic $[Pt_3(CO)_3(\mu_2\text{-}CO)_3]_4^{2-}$ shows a red shift by approximately 36 cm^{-1} (1860 → 1824 cm^{-1}), while the terminal CO band is blue-shifted about 40 cm^{-1} (2040 → 2080 cm^{-1}) with respect to those of crystalline $[Pt_3(CO)_3(\mu_2\text{-}CO)_3]_4^{2-}$ (Tables 1 and 2).[13−15] These shifts are consistent with the fact that the clusters interacted strongly with the extraframework Na^+ cations of the zeolite cages rather than the cluster on the MgO surface. The direction and magnitude of the band shifts are in agreement with the pattern of shifts observed from ion-paired metal carbonyl anions in solution. For example, the shifts of the terminal and bridging CO bands observed in $[Pt_3(CO)_3(\mu_2\text{-}CO)_3]_4^{2-}/N_{56}Y$ are analogous to the shifts observed from $[(C_5H_5)Fe(CO)_2]_2$ in solution containing AlR_3 (R = alkyl).[25] Similar shifts have been also observed for zeolitic $[Co_4(CO)_{12}]$,[3] $[Co_6(CO)_{16}]$,[8] and $[Ru_6(CO)_{18}]^{2-}$.[9] The magnitude of the shifts depends on the strength of ion-pairing. The basicity of the oxygen in CO ligands of metal carbonyl clusters depends on the CO coordination geometry; bridging CO ligands are significantly more basic than terminal CO ligands.[26] This pattern is borne out in the present results. The relatively large shift characteristic of the bridging CO band of $[Pt_3(CO)_3(\mu_2\text{-}CO)_3]_4^{2-}/Na_{56}Y$ suggests a strong interaction of the oxygen in bridging CO ligands of the $[Pt_3(CO)_3(\mu_2\text{-}CO)_3]_4^{2-}$ mainly with extraframework Na^+ cations. Such an interaction is expected to cause a net electron withdrawal from the cluster, which results

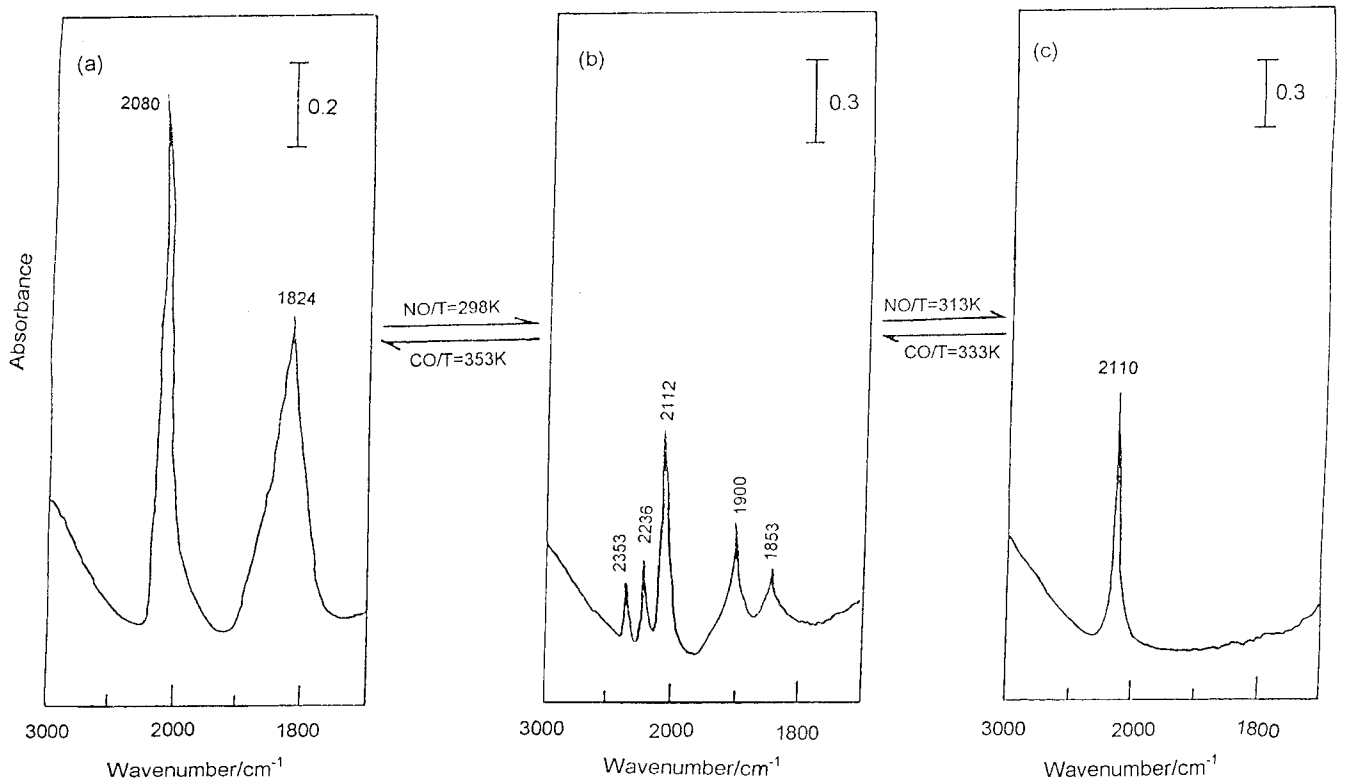

Figure 8. In situ infrared spectra characterizing the interaction of $[Pt_3(CO)_3(\mu_2\text{-}CO)_3]_4^{2-}/Na_{56}Y$ with 150 Torr of NO: (a) $[Pt_3(CO)_3(\mu_2\text{-}CO)_3]_4^{2-}/Na_{56}Y$ in a vacuum; (b) $[Pt_3(CO)_3(\mu_2\text{-}CO)_3]_4^{2-}/Na_{56}Y$ under150 Torr of NO at 298 K for 2 h; (c) $[Pt_3(CO)_3(\mu_2\text{-}CO)_3]_4^{2-}/Na_{56}Y$ under 150 Torr of NO at 313 K for 2 h and then evacuated at 298 K for 5 min.

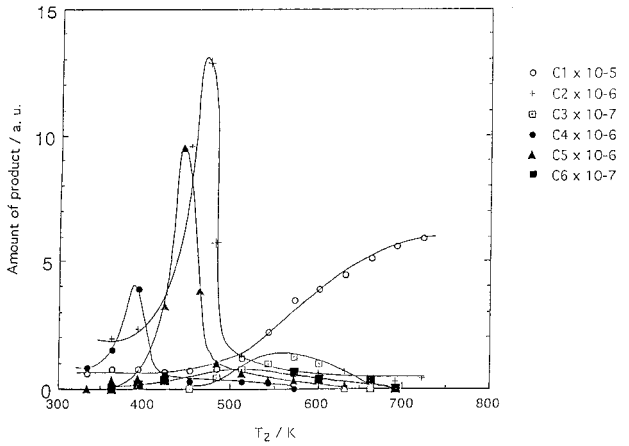

Figure 9. Temperature-programmed hydrogenation (TPH) plots of the surface carbonaceous deposits created from 20 μmol CH_4 dissociation on $[Pt_{12}]_{red}/Na56Y$ catalyst at 623 K.

TABLE 3: Kinetic Parameters for Methane Homologation on the Intra-zeolite Anchoring of Pt Cluster Catalyst[a]

hydrocarbon	optimum temp/K	selectivity/%[b]
C_2	473	67.8
C_3	573	1.8
C_4	393	43.2
C_5	453	17.6
C_6	573	1.1

[a] 100 mg $[Pt_x]_{dec}/Na_{56}Y$ (12 wt %); step 1: exposure of the catalyst to 20 μmol CH_4 at 623 K; step 2: hydrogenation of adspecies by a flow of H_2 (20 cm^3 min^{-1}, 1 atm). [b] C_{2+} selectivity $= \sum nC_n$ $(n = 2-6)/\sum nC_n$ $(n = 1-6)$.

in a decrease of the antibonding to the terminal CO ligands. Thereby, the result is a strengthening of the carbon−oxygen bond and a shift of the terminal CO bands to higher frequencies.

In contrast with the direction of infrared band shifts of the zeolitic $[Pt_3(CO)_3(\mu_2\text{-}CO)_3]_4^{2-}$, another zeolitic $[Pt_3(CO)_3(\mu_2\text{-}CO)_3]_3^{2-}$ species in sample a showed the bridging CO band at 1860 (s) cm^{-1}, which shifted from 1810 (s) cm^{-1} for free $[Pt_3(CO)_3(\mu_2\text{-}CO)_3]_3^{2-}$, while the terminal CO bands shifted from 1840 to 1894 cm^{-1}, and from 2030 to 2112 cm^{-1} (Tables 1 and 2). A tentative explanation is that under synthetic conditions, the $[Pt_3(CO)_3(\mu_2\text{-}CO)_3]_3^{2-}$ species interacted with surrounding water in zeolite α-cages. The H_2O with an abundant electron density will tend to donate electrons to 1π and/or 5σ orbital of CO ligands of $[Pt_3(CO)_3(\mu_2\text{-}CO)_3]^{2-}$ and would increase the carbon−oxygen bond, accompanied by the blue shifts of ν_{CO}.

Ramamurthy et al.[27] reported spontaneous electron transfer in which the "guest", upon inclusion within an activated zeolite, transfers an electron to the zeolite to form a stable radical cation. Jelinek et al.[28] provided insight into the interactions between the extraframework Na^+ cations and the adsorbed "guest" molecules by ^{23}Na DOR (double rotation) NMR spectra. Introduction of metal carbonyl guest into the cavities of faujasite causes a downshift of the resonance of site II ^{23}Na (α-cage). No appreciable band variation of the ^{23}Na resonance was observed, ascribed to the site I′ (β-cage) and site I Na^+ cations (hexagonal prism). These observations, together with our infrared band shifts of the $[Pt_3(CO)_3(\mu_2\text{-}CO)_3]_4^{2-}$ encapsulated in the zeolite cages, lead one to propose that a strong anchoring interaction occurs between the "guests" and the Na^+ cations at site II in the α-cage, through involvement of the oxygen end of the bridging ligands. The stereo and volume-filling requirements of the α-cage encapsulated $[Pt_3(CO)_3(\mu_2\text{-}CO)_3]_4^{2-}$ favor the four *trans*-ZONa- - -$(\mu_2$-OC$)Pt_2$ skeleton, having distorted D_{3h} symmetry involving four Na^+ site II cations (recall that there are four extraframework Na^+ site II cations per α-cage)[23,29] (Figure 6, part A, a), where Z = zeolite and O = lattice oxygen inside zeolite.

3. Distribution of the "Guest" in the "Host". The present experimental value of six molecules of $PtCl_2$ per unit cell is lower than the full coverage of $PtCl_2$ in cavities. Similar experiments with groups II−VI and IV−VI metal chalcogenides also showed lower coverage.[30] This is mainly ascribed to the special nanoporous structure and the internal heterogeneity of $Na_{56}Y$ zeolite. For example, the oxide framework of $Na_{56}Y$ is considered to be a macrospheroidal, multisite, and multidentate "zeolate" ligand[30] and may be unfavorable to the dynamic diffusion of $PtCl_2$.

A 12wt % Pt loading corresponds to 6 Pt ions/unit cell; therefore, one $[Pt_3(CO)_3(\mu_2\text{-}CO)_3]_4^{2-}$ per two unit cells was synthesized in sample b. Often it is assumed that there is a uniform distribution of "guest" molecules among the cavities of the zeolite. However, few physical techniques have been reported that can actually differentiate between the distinct types of molecular dispersions that can exist. Only recently have elegant xenon-129 and multiple quantum NMR experiments been able to provide a rather direct and informative picture of the heterogeneous distribution of metal compounds among the cavities of the zeolite.[31] In the present study, a stoichiometric, intrazeolite "acid−base titration" of Pt carbonyl dianions with extraframework Na^+ α-cage cations can be considered as a *chemical probe* of the distribution in the case of maximum loading of one "guest" per 16 α-cages. The reactivity of $[Pt_3(CO)_3(\mu_2\text{-}CO)_3]_4^{2-}$ with the respect to Na^+ cations of α-cages is expected to impede further diffusion of Pt^{2+} ions into empty α-cages deep in the zeolite crystal. Thus, the "guests" are suggested to be located in the α-cages in regions close to the external surface of zeolite.

4. Chemical Reactivity of the Intra-zeolitic Platinum Carbonyl Dianion Clusters. The chemistry of $Na_{56}Y$ zeolitic platinum carbonyl dianions includes that the reductive carbonylation of Pt^{2+} within $Na_{56}Y$ cavities under CO atmosphere which formed a high yield $[Pt_3(CO)_3(\mu_2\text{-}CO)_3]_4^{2-}$. However, under a mixed CO and H_2O atmosphere, a mixture of $[Pt_3(CO)_3(\mu_2\text{-}CO)_3]_4^{2-}$ and $[Pt_3(CO)_3(\mu_2\text{-}CO)_3]_3^{2-}$ was formed. For sample b, the pattern of reaction accords to the following stoichiometric equation:

$$12Pt^{2+}/Na_{56}Y + 24CO \rightarrow [Pt_3(CO)_3(\mu_2\text{-}CO)_3]_4^{2-}/Na_{56}Y \quad \text{(i)}$$

The formation of $[Pt_3(CO)_3(\mu_2\text{-}CO)_3]_3^{2-}$ in sample a is consistent with reaction eq ii:

$$9Pt^{2+}/Na_{56}Y + 19CO + H_2O \rightarrow [Pt_3(CO)_3(\mu_2\text{-}CO)_3]_3^{2-}/Na_{56}Y + 2H^+/Na_{56}Y + CO_2 \quad \text{(ii)}$$

The oxidation of water is concomitant with the reduction of Pt species during the clusters formation. The platinum carbonyl dianions in organic solution display a competition between reduction by CO and H_2O and reverse oxidation by the corresponding free protons. However, the protons produced here bind to the framework oxygen of zeolite, forming an OH group inside the cavities, which was detected through infrared peaks at 3654 cm^{-1} (occurring inside the α-cages)[9] (Figure 2, part A, traces a−i), and 3556 cm^{-1} (occurring at small cativities)[9] (Figure 2, part A, traces e−i). The peak intensities of bridged hydroxyl increased with the synthesis of Pt carbonyl dianion clusters. This suggests that the reaction ii is irreversible, and unlike their solution chemistry. The formed CO_2 gas phase can also be detected through an infrared frequency at 2360 cm^{-1} (Figure 2, part B). The reducing behavior of Chini dianion clusters, i.e., conversion of the Pt_{12} cluster to the Pt_3 carbonyl cluster, was described as H_2O introduced to the system.[15] This conversion was also observed in Figure 2, part B, which accompanied the oxidation of CO ligands, presumably by nucleophilic attack of H_2O on coordinated CO groups to form CO_2 and H^+. Thereby, $[Pt_3(CO)_3(\mu_2\text{-}CO)_3]_3^{2-}$ is also considered to create from $[Pt_3(CO)_3(\mu_2\text{-}CO)_3]_4^{2-}$ under a H_2O environment as eq iii:

$$3[Pt_3(CO)_3(\mu_2\text{-}CO)_3]_4^{2-}/Na_{56}Y + 2H_2O \rightarrow 4[Pt_3(CO)_3(\mu_2\text{-}CO)_3]_3^{2-}/Na_{56}Y + 4H^+/Na_{56}Y + O_2 \quad \text{(iii)}$$

The infrared spectrum of sample c (Figure 4, trace f), is attributed to a mixture of $[Pt_3(CO)_3(\mu_2\text{-}CO)_3]_4^{2-}$ and $[Pt_3(CO)_3(\mu_2\text{-}CO)_3]_3^{2-}$, with the dodecaplatinum carbonyl dianions being 80%. The ratio of the two dianion clusters was estimated from their area ratio of infrared CO bands. The observation of $[Pt_3(CO)_3(\mu_2\text{-}CO)_3]_3^{2-}$ is ascribed to the reduction of $[Pt_3(CO)_3(\mu_2\text{-}CO)_3]_4^{2-}$ by H_2, according to the following equation:

$$3[Pt_3(CO)_3(\mu_2\text{-}CO)_3]_4^{2-}/Na_{56}Y + H_2 \rightarrow 4[Pt_3(CO)_3(\mu_2\text{-}CO)_3]_3^{2-}/Na_{56}Y + 2H^+/Na_{56}Y \quad \text{(iv)}$$

The produced protons bind to the framework oxygen of zeolite, preventing the reversal reduction of protons in eq iv. The reactions iii and iv are consistent with the reactivity tend of $[Pt_3(CO)_3(\mu_2\text{-}CO)_3]_n^{2-}$ in organic solution, which is that decreasing *n* results in an increase in reactivity toward electrophiles and oxidizing agents.[14,15]

$[Pt_3(CO)_3(\mu_2\text{-}CO)_3]_4^{2-}$ is converted to PtO(CO) species through the intermediate $[Pt_3(CO)_3(\mu_2\text{-}CO)_3]_3^{2-}$ under a NO atmosphere. CO_2 was produced in the conversion, which showed by infrared spectrum at 2353 cm^{-1} (Figure 8, part b). The CO_2 was considered to occur from the nucleophilic attack of NO on coordinated CO groups. The intensity of the band at 2110 cm^{-1} increased with increasing reaction time (Figure 8, part c). In addition, PtO(CO) can be recarbonylated under a CO atmosphere at 353 K, and infrared bands show the reformation of $[Pt_3(CO)_3(\mu_2\text{-}CO)_3]_4^{2-}$. This reversible process is illustrated in eq v:

$$[Pt_3(CO)_3(\mu_2\text{-}CO)_3]_4^{2-}/Na_{56}Y \underset{CO}{\overset{NO}{\rightleftharpoons}} [Pt_3(CO)_3(\mu_2\text{-}CO)_3]_3^{2-}/Na_{56}Y \underset{CO}{\overset{NO}{\rightleftharpoons}} PtO(CO)/Na_{56}Y \quad \text{(v)}$$

Chang et al.[32] reported that the successful synthetic condition of the 3 wt % zeolitic Pt carbonyl dianion clusters was the introduction of CsOH of zeolite to enhance the basicity of zeolite. Li et al.[18] prepared 4 wt % $[Pt_3(CO)_3(\mu_2\text{-}CO)_3]_3^{2-}$ in $Na_{56}Y$ zeolite cages. They used the precursor from the ion exchange of $Pt(NH_3)_4Cl_2$ with Na^+ cations of $Na_{56}Y$ zeolite in solution with pH = 8.9. The Na^+ cations were exchanged out of zeolite, which resulted in the decrease of the solid-state basicity of zeolite. The pretreatment of NaY with CsOH as well as the basic solution of exchange Na^+ is considered to compensate for the basicity of the of $Na_{56}Y$ zeolite. The present $PtCl_2$ vaporous chemistry within zeolite cavities remained the solid-state basicity of zeolite, being consistent with the above examples. By contrast, platinum on HY or NH_4Y cavities does not give the infrared bands or the bright color of Chini dianion clusters.[13,14] The zeolitic acidic character would harm the formation of Chini dianion clusters in their cages. Thus, we can say that the sufficient base strength of $Na_{56}Y$ zeolite provides an efficient medium to favor the formation of Chini

dianion clusters. This is consistent with the inference that the interaction of the metallic ions with a basic support results in an increase in the electron density on metallic ions which promote the formation of multinuclearity metal.[33]

Experimental Section

1. Sample Preparation. *$Pt^{2+}/Na_{56}Y$ Precursor*. The dispersion of $PtCl_2$ vapor in $Na_{56}Y$ cavities (12 wt % Pt loading or 6 Pt atoms/unit cell) was prepared by heating a mixture of $PtCl_2$ (Strem Chemical) with $Na_{56}Y$ zeolite powder (HSZ-320NAA, Lot No. D1-9915, Si/Al = 2.8, surface area 910 m^2/g). The $Na_{56}Y$ zeolite powder was dehydrated by evacuation at 623 K for 2 h and then mixed mechanically with $PtCl_2$ under a N_2 atmosphere at 300 K, followed by careful heating in a vacuum at 473 K for 98 h to give the light-brown sample denoted as precursor $Pt^{2+}/Na_{56}Y$.

Sample a. $Pt^{2+}/Na_{56}Y$ was exposed to 550 Torr of CO and 15 Torr of H_2O in a closed circulation system and heated from 298 to 353 K. After 8 h, the apparent color of the carbonylated sample changed from light brown to dark green and showed stable infrared carbonyl stretching frequencies; it is denoted as sample a.

Sample b. $Pt^{2+}/Na_{56}Y$ was exposed to 550 Torr of CO in a closed circulation system and heated from 298 to 353 K. After 8 h, the apparent color of the carbonylated sample changed from light brown to blue-green and showed stable infrared carbonyl stretching frequencies; it is denoted as sample b.

Sample c. 100 Torr of H_2 was introduced to sample b and heated from 298 to 373 K.

Sample b was decarbonylated under 10^{-5} Torr vacuum at heating by 5 K/min to 423 K and then kept at 423 K for 30 min. The decarbonylated sample b is denoted as $[Pt_x]_{dec}/Na_{56}Y$.

The concentration of Pt in samples a and b was determined using an inductively coupled plasma atomic emission (ICP) spectrometer. Attempts to extract organometallic species from samples a and b were performed through a solution of *n*-Bu4NBr in acetone.

2. Characterization of Samples. *Infrared Spectroscopy*. In situ spectra of the samples were recorded with a Shimadzu infrared 4200 double-beam spectrometer with 20−100 co-added scans at 2 cm^{-1} resolution. The sample was pressed into a self-supporting wafer (8 mg cm^{-2}) in a N_2 atmosphere box and mounted in a quartz infrared cell with CaF_2 windows connected to a vacuum closed-circulating Pyrex glass line (10^{-5} Torr). The infrared cell was equipped with an electric heater and a liquid N_2 reservoir for high- and low-temperature measurements. The contribution of the gas phase was compensated by using a reference infrared cell having the same optical length as the sample cell. In situ infrared spectra recorded the preparation of samples a, b, and c. CO chemisorption on $[Pt_x]_{dec}/Na_{56}Y$, ^{13}CO isotopic exchange, and NO reactions were performed in the infrared cell using enriched ^{13}CO (98% ^{13}CO and 99.9% NO) purchased from Merck Reagent Co. Ltd. Before use, all gases were passed through traps to remove water and/or oxygen.

Powder X-ray Diffraction and Gas Chromatography. The PXRD measurement was carried out using a MAS Science diffractometer with Cu Kα radiation (λ = 1.5418 Å). The gaseous products were determined using a Hewlett-Packard 5992 GC-MS.

3. Methane Homologation. A hundred milligrams of decarbonylated sample was placed in the reactor and was flushed with He at 300 K for 30 min. The temperature was raised under flowing He. The procedure was switched to a pulsed gas containing dilute CH_4 in He for methane decomposition when the temperature reached to 623 K. After methane dissociation, the catalyst was quickly cooled to room temperature under He flowing to avoid aging of the surface carbonaceous deposits. The surface carbonaceous species were subsequently hydrogenated in H_2 flow of 20 cm^{-3}/min from 298 to 723K. Before they entered the catalyst bed, the gases (He, CH_4, and H_2) were purified with manganese oxide and molecular sieve. The effluent gases from the reactor were stored in the loops and were determined afterward by Shimadzu GC-8A gas chromatography with a flame ionization detector.

References and Notes

(1) *Metal Cluster in Catalysis*; Gates, B. C., Guczi, L., Knozinger, H., Eds.; Elsevier: Amsterdam, 1986.
(2) Shen, J. G. C.; Ichikawa, M. *J. Phys. Chem. B* **1998**, *102*, 5602.
(3) Shen, J. G. C.; Liu, A. M.; Tanaka, T.; Ichikawa, M. *J. Phys. Chem. B* **1998**, *102*, 7782.
(4) Shen, G. C.; Ichikawa, M. *J. Chem. Soc., Faraday Trans*. **1997**, *93*, 1185.
(5) Shen, G. C.; Liu, A. M.; Shido, T.; Ichikawa, M. *Top. Catal*. **1995**, *2*, 141.
(6) Rao, L. F.; Fukuoka, A.; Kosugi, N.; Kuroda, H.; Ichikawa, M. *J. Phys. Chem*. **1990**, *94*, 5317.
(7) Kawi, S.; Chang, J. R.; Gates, B. C. *J. Am. Chem. Soc*. **1993**, *115*, 4830.
(8) Shen, G. C.; Ichikawa, M. *J. Phys. Chem*. **1996**, *100*, 16947.
(9) Shen, G. C.; Liu, A. M.; Ichikawa, M. *Inorg. Chem.* **1998**, *37*, 5497.
(10) Shen, G. C.; Ichikawa, M. *J. Phys. Chem*. **1996**, *100*, 14265.
(11) *Oil Gas J*. **1992**, *190*, 29.
(12) Rotman, D. *Chem. Week* **1992**, *150*, 8.
(13) Calabrese, J. C.; Dahl, L. F.; Cavalieri, A.; Chini, P.; Longoni, G.; Martinengo, S. *J. Am. Chem. Soc*. **1974**, *96*, 2614.
(14) Longoni, G.; Chini, P. *J. Am. Chem. Soc*. **1976**, *98*, 7225.
(15) Basu, A.; Bhaduri, S.; Sharma, K. R. *J. Chem. Soc., Dalton Trans.* **1984**, 2315.
(16) Efremov, A. A.; Bakhmutova, N. I.; Pankratiev, Yu. D.; Kuznetsov, B. N. *React. Kinet. Catal. Lett*. **1985**, *28*, 103.
(17) Grill, C. M.; McLauglin, M. L.; Stevenson, J. M.; Gonzalez, R. D. *J. Catal*. **1981**, *69*, 454.
(18) Li, G. J.; Fujimoto, T.; Fukuoka, A.; Ichikawa, M. *Catal. Lett.* **1992**, *12*, 171.
(19) Puga, J.; Patrini, R.; Sanchez, K. M.; Gates, B. C. *Inorg. Chem*. **1991**, *30*, 2479.
(20) Anderson, G. K.; Clark, H. C.; Davis, J. A. *Inorg. Chem*. **1981**, *20*, 1636.
(21) Calderazo, F.; Dell'Amico, D. B. *Inorg. Chem*. **1981**, *20*, 1310.
(22) Primet, J. *J. Catal*. **1984**, *88*, 273.
(23) Breck, D. W. *Zeolite Molecular Sieves*; Wiley: New York, 1974.
(24) DeMallmann, A.; Barthomeuf, D. *Catal. Lett*. **1990**, *5*, 293.
(25) Shriver, D. F. *J. Organomet. Chem*. **1975**, *94*, 259.
(26) Lamb, H. H.; Gates, B. C.; Knözinger, H. *Angew. Chem., Int. Ed. Engl*. **1988**, *27*, 1127.
(27) Ramamurthy, V.; Lakshminarasimhan, P.; Grey, C. P.; Johnston, L. J. *J. Chem. Soc., Chem. Commun.* **1998**, 2411.
(28) Jelinek, P. Ph.D. Thesis, Department of Chemistry, University of Toronto, 1993.
(29) Ozin, G. A. Gil, C. *Chem. Rev*. **1989**, *89*, 1749.
(30) Ozin, G. A. In *Materials Chemistry*; Interrance, L. V., Casper, L. A., Ellis, A. B., Eds.; American Chemistry Society: Washington, DC, 1995; pp 335−371.
(31) Ryoo, R.; Liu, S. B.; de Menorval, L. C.; Takegoshi, K.; Chmelka, B.; Trecoske, M.; Pines, A. *J. Phys. Chem*. **1987**, *91*, 6575.
(32) Chang, J. R.; Xu, Z.; Purnell, S. K.; Gates, B. C. *J. Mol. Catal*. **1993**, *80*, 49.
(33) Miller, J. T.; Modica, F. S.; Meyers, B. L.; Koningsberger, D. C. *Prepr.—Am. Chem. Soc., Div. Pet. Chem.* **1993**, *38*, 825.